J Appl Electrochem (2007) 37:575–582
DOI 10.1007/s10800-006-9288-7

ORIGINAL PAPER

Electrodeposition of copper–magnetite magnetic composite films

A. Roldan · E. Gómez · S. Pané · E. Vallés

Received: 28 September 2006 / Accepted: 14 December 2006 / Published online: 20 January 2007

Abstract Electrodeposition was demonstrated to be useful for the preparation of copper–magnetite magnetic composites. An acidic bath was tested for the incorporation of nanometric magnetite (Fe_3O_4) particles into an electrodeposited copper matrix. Cationic surfactant (dodecyltrimethylammonium chloride—DTAC) was used to keep particles suspended in the electrolyte as well as to assist magnetite incorporation. The influence of several parameters (bath temperature, deposition technique, stirring regimes and deposition conditions) on composites composition was analysed. Low stirring rate, moderate temperature (15 °C) and an applied magnetic field provided a greater incorporation of magnetite. Field emission scanning electron microscopy revealed magnetite distribution through the deposit thickness. Electrodeposited composites showed ferromagnetic behaviour. Magnetic force microscopy showed a magnetic response for the composites.

Keywords Composite · Electrodeposition · Magnetic properties · Copper · Magnetite

1 Introduction

Nanostructured materials have been attracting much attention during recent years due to novel properties of the nanostructures, which are noticeably different from the corresponding bulk materials with similar composition [1–5]. There is an extensive interest in the preparation of composites with particles of different nature. Magnetic solids, consisting of ferromagnetic particles embedded immiscibly in a matrix, have been studied in recent years [6–10], especially for magnetic applications. Most of these granular solids consisted of magnetic particles embedded in an insulating material such as a silica or alumina matrix [10–13]. On the other hand, magnetic materials containing magnetic oxides dispersed in a metallic matrix [6, 10, 14] have also been developed. The properties of these systems strongly depend on the size and distribution of particles.

Many chemical and physical methods have been developed to prepare particle–metal composites but most of them are expensive. Electrolytic codeposition of particles with a metal matrix is a low-cost technique to prepare composites [15–18]. The aim of the present study is to determine the possibility of electrodeposition for the preparation of magnetic composites consisting of magnetic nanoparticles embedded into a metallic matrix. The level of incorporation of the particles and their distribution in the matrix will be analysed.

The preparation of a composite consisting of magnetic oxide nanoparticles (magnetite, Fe_3O_4) embedded into a ductile metallic matrix (Cu) is reported. Copper–magnetite composites have been previously prepared by ball-milling copper oxide and iron under argon [6], by Fe(II) disproportionation in basic media and simultaneous Cu(II) reduction [19] or RF-sputtering [20]. The aim of the current work is to produce copper–magnetite composites by working at low temperature and at normal pressure. Different electrodeposition conditions will be tested to control

A. Roldan · E. Gómez · S. Pané · E. Vallés (✉)
Electrodep, Departament de Química Física and Institut de Nanociència i Nanotecnologia, Universitat de Barcelona, Martí i Franquès 1, 08028 Barcelona, Spain
e-mail: e.valles@ub.edu

the incorporation of magnetite into the deposit. Simultaneously, the particles distribution in the matrix and structural and magnetic properties of the composites will be analysed.

2 Experimental details

Electrochemical experiments were performed in a cylindrical three-electrode cell of 0.25 dm^3 with termostatization. Solutions contained $CuSO_4$, H_2SO_4 and cationic surfactant (dodecyltrimethylammonium chloride—DTAC), all of analytical grade. Copper (II) was maintained at 0.5 mol dm^{-3} in 0.2 mol dm^{-3} H_2SO_4. In order to keep magnetite suspended in the electrolyte and to favour particles incorporation into the deposits, DTAC concentration was varied between 1 and 20 g dm^{-3}. Nanometric magnetite particles were synthesized. High concentrations of magnetite (25–50 g dm^{-3}) were tested. Temperature of the bath was varied between 15 and 30 °C. Solutions were freshly prepared with water which was first distilled twice and then treated with a Millipore Milli Q system. Solutions were de-aerated by argon bubbling before each experiment. Argon atmosphere was maintained during experiments.

A microcomputer-controlled potentiostat/galvanostat Autolab with PGSTAT30 equipment and GPES software has been used to the experiments. Silicon/Ti(1000 Å)/Ni(500 Å) substrates supplied by IMB-CNM. Centro Nacional de Microelectrónica (CSIC) were used as working electrodes. The silicon-based substrates were cleaned with acetone followed by ethanol and rinsed in water before deposition. The reference electrode was an Ag/AgCl/1 mol dm^{-3} NaCl electrode mounted in a Luggin capillary containing 0.5 mol dm^{-3} Na_2SO_4 solution. All potentials are referred to this electrode. Copper rod or platinum spiral was used as counter electrode.

Voltammetric experiments were carried out under quiescent or stirring conditions at 50 mV s^{-1}, scanning initially from 0 mV towards negative potentials. A single cycle was run in cyclic voltammetric experiments. Different electrochemical deposition techniques were tested in the preparation of deposits: galvanostatic, potentiostatic or pulse-plating techniques.

Scanning electron microscopes (Hitachi S 2300, Leica Stereoscan S-360) have been used to analyse surface morphology and deposit section. Field Emission scanning electron microscope (FE-SEM) (Hitachi S-4100) was used in some cases. For the cross-section preparation, samples were resin-encased in a mould and accurately polished. Polishing papers of different grain size were used for initial preparation of the sections. After, deposits were polished with alumina of 6, 1 and 0.3 μm suspended in distilled water in order to attain a good observation of the cross-section without damage of the deposit.

Deposits composition was determined by inductively coupled plasma optical emission spectrometry (ICP-OES) with a Perkin-Elmer Optima 3200 RL. Aqua regia was used to dissolve the deposits.

Structural analysis of the synthesised magnetite was performed by means of X-ray diffraction (XRD) equipment (Siemens D-500). Diffractograms were obtained in the 10–100° 2θ range with a step range of 0.03° and a measuring time of 8 s per step. Structural analysis of the composites was performed in the 5–100° 2θ range with a step range of 0.05° and a measuring time of 30 s by step.

Magnetic measurements were taken in a magnetometer (SQUID Quantum Design MPMS XL) at room temperature. Magnetic force microscopy (MFM) measurements were performed with a multimode atomic force microscope (AFM) (Veeco Instruments, CA, USA) controlled by a Nanoscope IIIa electronics (Veeco Instruments, CA, USA). Co–Cr magnetic probes (MESP probes, Veeco Instruments, CA, USA), were employed for magnetic detection. Magnetic maps were measured through the MFM phase signal recorded at a lift distance of 150 nm above the sample surface in order to minimize topographic components. The lift distance was greater than the sample roughnesses which were measured by means of Nanoscope IIIa software.

3 Results and discussion

3.1 Preparation and characterization of the magnetite

Magnetite (Fe_3O_4) was prepared by means of chemical precipitation from solutions containing $FeSO_4 \cdot 5H_2O$ (13 g dm^{-3}) and NaOH (9.2 g dm^{-3}) in the presence of $NaNO_3$ at high temperature (90 °C) and stirring of solution. After filtration, a high yield (up to 80%) was obtained.

When synthesized magnetite was analysed by using FE-SEM, agglomerates of rounded nanometric particles were observed (Fig. 1A). X-ray diffraction pattern of particles powder showed (Fig. 1B) a group of peaks corresponding to the crystalline spinel structure of the magnetite; two small peaks (21.2°, 33.3° 2θ) assigned to orthorhombic goethite; and other two small peaks (14.1° and 27.1° 2θ) corresponding to orthorhombic

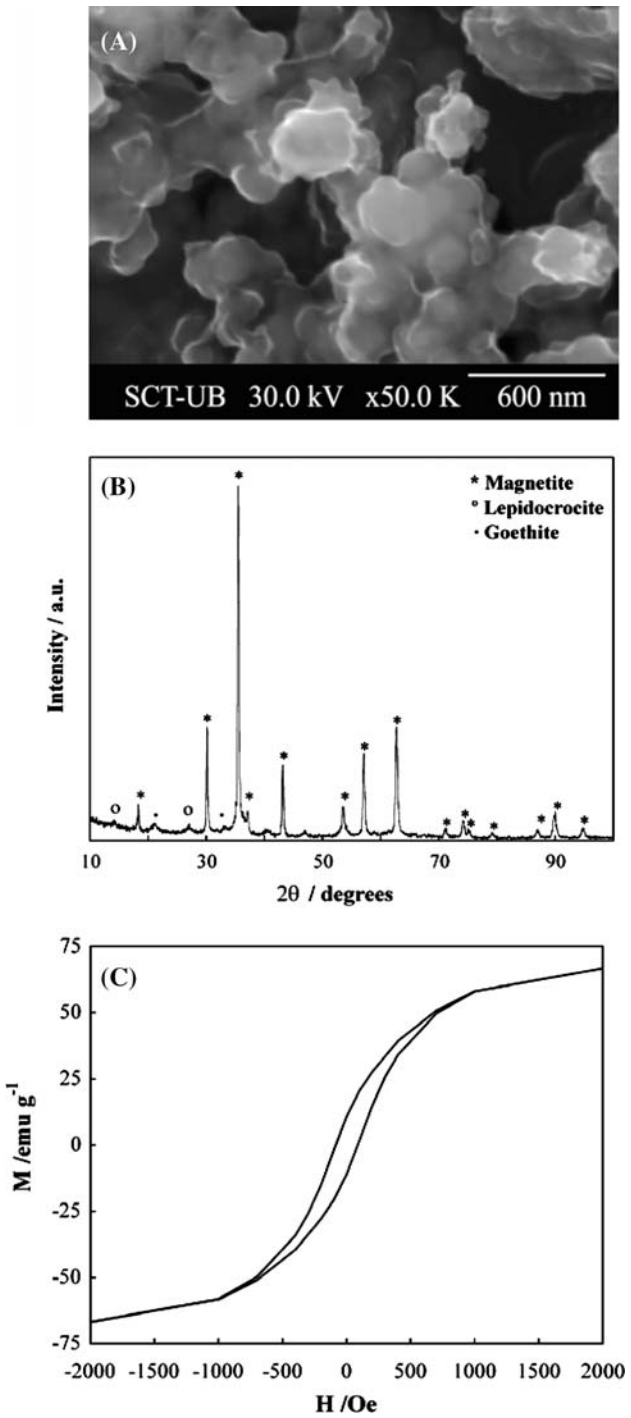

Fig. 1 (**A**) FE-SEM image at 50 kX of the synthesised magnetite. (**B**) X-ray diffractogram of the synthesised magnetite. (**C**) Magnetization versus magnetic field for the synthesised magnetite

lepidocrocite. Diffractograms revealed that the preparation method led mainly to magnetite, although a very small amount of iron oxide hydroxide (FeO(OH)) was simultaneously formed.

Diffraction peaks corresponding to magnetite were wide. The estimation of the crystallite size domain was obtained from X-ray line broadening by using Scherrer's equation. From the full width at half maximum (FWHM) of the reflection peaks, a particle-size ranged between 20 and 30 nm was obtained.

Figure 1C shows the magnetization versus magnetic field curve which corresponded to the expected ferromagnetic response of magnetite particles. Saturation magnetization of 83 emu g^{-1} and coercivity of 85 Oe were obtained.

3.2 Electrodeposition of copper–magnetite coatings

The XRD study of the magnetite particles after being in contact with the bath during deposit preparation revealed that these particles were stable in the electrolyte and were maintained as ferromagnetic magnetite.

Different parameters (bath composition, temperature, hydrodynamic conditions and the presence of a magnetic field during the deposition process) were systematically studied. The influence of either the deposition potential or the current density in each case was analysed. Parallel experiments were run from a free-magnetite bath in order to compare the composites with the pure-copper deposits.

With the aim of establishing hydrodynamic conditions, previous experiments were run by varying the stirring rate from 0 to 700 rpm. It was demonstrated that high stirring rates did not facilitate the inclusion of nanoparticles into the copper deposits. Moderate stirring rates not only were enough to keep magnetite nanoparticles suspended in the electrolytic bath in the presence of the cationic surfactant, but they were more adequate when a high incorporation of particles is desired. Most of the experiments were performed at a stirring rate of 60 rpm. Moreover, the bath was maintained in all cases under stirring conditions during one hour previously to deposits preparation.

Figure 2 shows the voltammetric curves obtained at two different temperatures for one of the tested conditions. As expected, an increase of temperature shifted the onset of copper deposition to more positive potentials. Simultaneously, higher intensity of the reduction peak was detected as a consequence of the increase of the diffusion coefficient with temperature. A high value of the Q_{ox}/Q_{red} (ratio between oxidation and reduction charge) was obtained in all cases, revealing that the electrodeposited copper is almost oxidized when the voltammetric scan is completed.

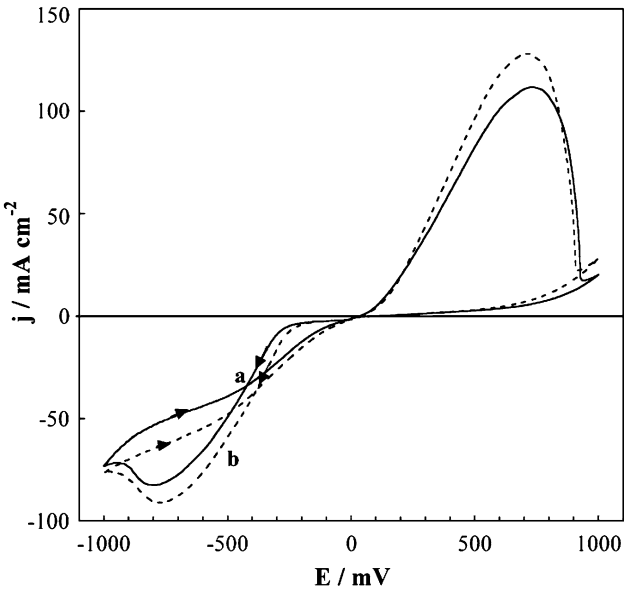

Fig. 2 Cyclic voltammetry of a 0.5 mol dm^{-3} $CuSO_4$ + 0.2 - mol dm^{-3} H_2SO_4 + 1 g dm^{-3} DTAC + 25 g dm^{-3} Fe_3O_4 solution at (a) 15 °C and (b) 30 °C. Cathodic limit: –1000 mV, ω = 60 rpm, 50 mV s^{-1}

From the voltammetric curves, a set of potentials useful to electrodeposit the composites was selected. Some deposits were prepared potentiostatically ranging between –400 and –900 mV. Potential values more negative than –700 mV were required to promote particles incorporation. When deposits were prepared by means of galvanostatic technique, a wide range of current densities (–3 to –60 mA cm^{-2}) was tested.

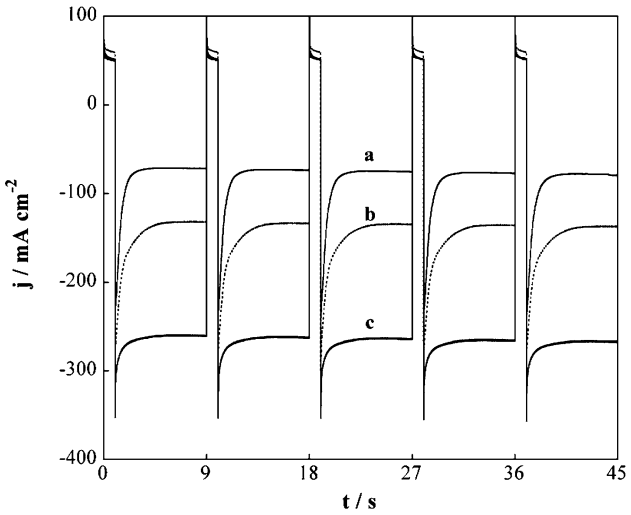

Fig. 3 j versus t transients at ω = 60 rpm during pulse application from the same solution of Fig. 2. E_c = –850 mV, t_c = 8 s, E_a = 200 mV, t_a = 1 s. (a) 15 °C, (b) 22 °C and (c) 30 °C

Particle incorporation was significant when applied current densities were sufficiently negative.

When deposits were prepared by pulse-plating, the deposition proceeds alternating deposition for a defined time (t_c) at a cathodic potential (E_c) and oxidation at an anodic potential (E_a) for a short time (t_a). Figure 3 shows the j–t transients during pulse-plating deposition at a fixed cathodic potential and at different temperatures. A gradual behaviour of the reduction transients as a function of temperature was observed.

Table 1 shows some weight percentages of entrapped magnetite in the copper deposits from different

Table 1 Amount of Fe_3O_4 (wt%) in Cu–magnetite deposits obtained by potentiostatic (p), galvanostatic (g) or pulse-plating (pp) method from a 0.5 mol dm^{-3} $CuSO_4$ + 0.2 mol dm^{-3} H_2SO_4 solutions with different DTAC and magnetite concentrations

Method	E_{red} (mV)	[Fe_3O_4] (g l^{-1})	[DTAC] (g l^{-1})	$-Q$ (C cm^{-2})	ω (rpm)	Magnetic field (G)	Temperature (°C)	wt% Fe_3O_4
pp	–650	50	20	6	60	–	15	0.2
pp	–700	50	20	7	60	–	15	0.3
pp	–750	50	20	6	60	–	15	0.4
pp	–800	50	20	7	60	–	15	0.4
pp	–850	50	20	6	60	–	15	0.2
pp	–900	50	20	6	60	–	15	0.2
pp	–850	50	2	7	60	350	15	8
pp	–850	50	2	15	60	350	15	3
pp	–850	50	2	34	60	350	15	4
pp	–850	25	1	10	60	350	15	12
pp	–850	25	1	22	60	350	22	3
pp	–850	25	1	25	60	350	30	2
p	–850	25	1	10	60	350	15	14
p	–850	25	1	30	60	350	15	17
pp	–850	50	1	5	60	350	15	6
pp	–850	50	1	18	60	350	15	8
pp	–850	50	1	43	60	350	15	11
pp	–850	50	1	8	0	350	15	0.7
g	–30	25	1	28	60	350	15	5
g	–60	25	1	67	60	350	15	32

For pp technique: E_{red} = x mV, t_{red} = 8 s, E_{ox} = 200 mV, t_{ox} = 1 s

deposition methods as a function of different parameters (bath temperature, electrochemical method, cationic surfactant concentration, magnetite concentration and deposited charge). All electrochemical methods used are suitable to incorporate magnetite in the deposit.

With the purpose of analysing the influence of a magnetic field, a magnet of 350 G attached behind the working electrode was used for several experiments. Incorporation of magnetic particles into the films was enhanced by electrodepositing at low temperature and by applying a magnetic field. About 25 g dm^{-3} Fe_3O_4 and low concentration of the surfactant (1 g dm^{-3}) in the solution were adequate for obtaining composites with high magnetite content. Moreover, at these conditions, a slight increase in magnetite percentage into deposits along the thickness was observed. It is supposed that higher DTAC concentrations inhibited copper (or composite) deposition due to the adsorption of free surfactant on the substrate or initial deposit. High percentages around 15–30 wt% can be attained by using different deposition methods.

3.3 Morphology and structure of copper–magnetite composites

SEM micrographs of different copper–magnetite composites were taken and compared with those corresponding to pure-copper deposits obtained from the same electrolyte at equivalent conditions. Copper deposits prepared by using potentiostatic, galvanostatic or pulse-plating methods in the presence of surfactant exhibited an edged morphology (Fig. 4A) whereas copper–magnetite composites showed a clearly different rough nodular morphology (Fig. 4B) as a consequence of magnetite incorporation.

Cross-sections of deposits were observed by means of SEM and analysed by EDS. Figure 5A shows the cross-section of Cu–magnetite (32 wt%) deposit observed by field-emission SEM. Uniform distribution of the magnetite is shown. The EDS local analysis confirmed the presence of magnetite along the all section of the composite (Fig. 5B).

Figure 6 shows X-ray diffraction patterns of copper and copper–magnetite films obtained from equivalent electrolytic baths. Copper films obtained in the presence of surfactant (Fig. 6A) are crystalline in nature and have fcc structure. In the diffractograms, a set of peaks corresponding to nickel and titanium of the substrate seed-layer also appear. When copper–magnetite composites were analysed by means of X-ray diffraction, a new peak centred at about 34.5° 2θ appears close to the peaks assigned to copper and the seed-layer (Fig. 6B). This peak

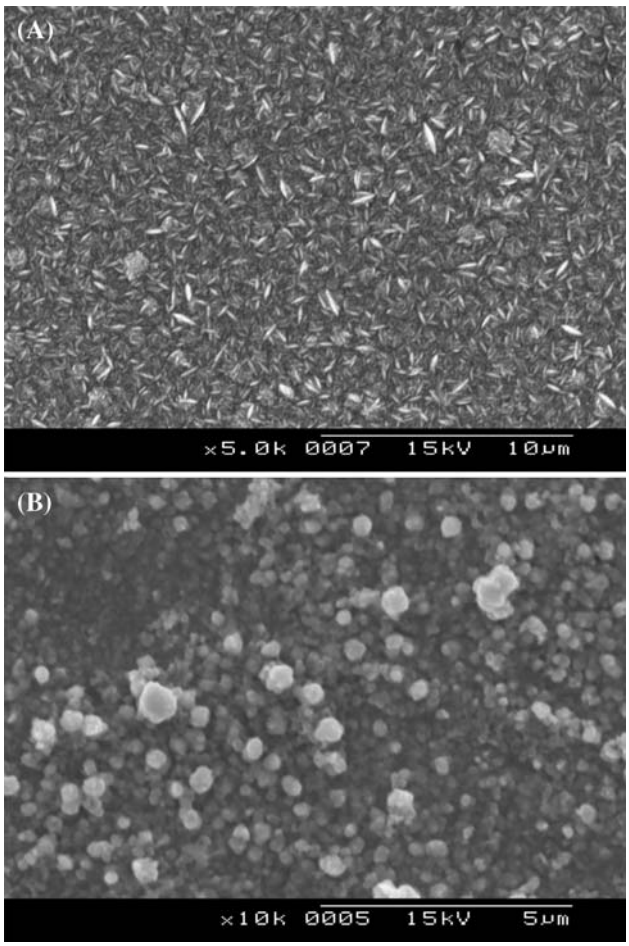

Fig. 4 SEM images of deposits obtained from a 0.5 mol dm^{-3} $CuSO_4$ + 0.2 mol dm^{-3} H_2SO_4 + 1 g dm^{-3} DTAC + (**A**) 0 g dm^{-3}, (**B**) 50 g dm^{-3} Fe_3O_4 solution at 15 °C, ω = 60 rpm, Q = –10 C cm^{-2}, magnet, using pulse-plating with E_c = –850 mV, t_c = 8 s, E_a = 200 mV, t_a = 1 s

appeared only for magnetite-containing deposits and corresponded to the predominant reflection (311) of a $Fe_{2.93}O_4$ magnetite of cubic spinel structure. No diffraction peaks corresponding to metallic iron, iron hydroxides or other iron oxides were detected. Therefore, it is confirmed that practically all the iron of the composite is in the form of non-reduced magnetite. Consequently, the iron content determined by ICP analysis allows quantifying magnetite incorporation.

3.4 Magnetic properties of copper–magnetite composites

Magnetization versus magnetic field curves (M vs. H) were registered in order to analyse the magnetic response for the deposits. Magnetic properties were

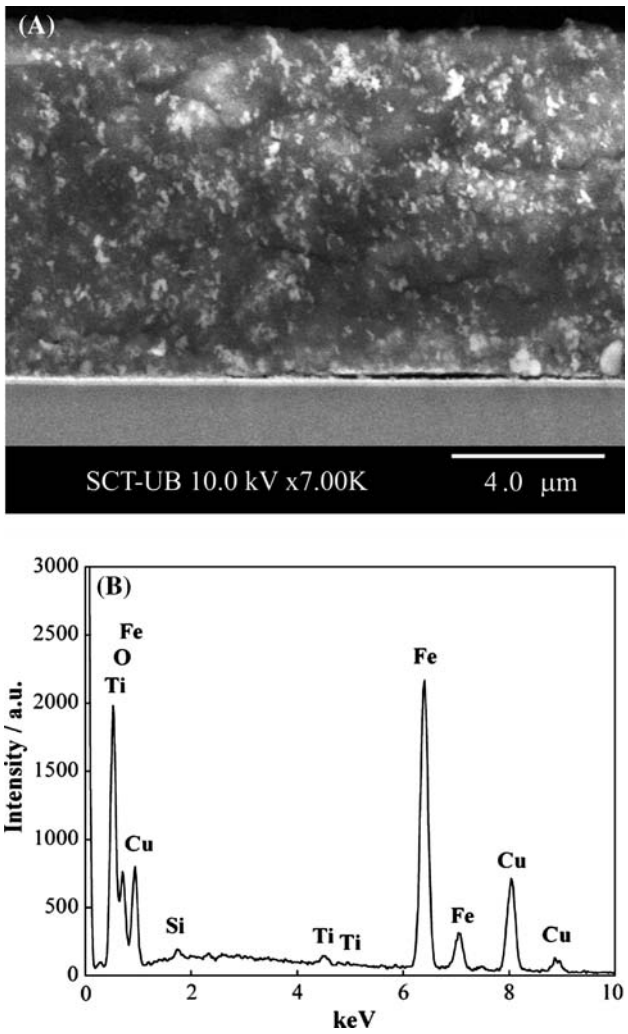

Fig. 5 (**A**) Cross-section SEM image of a Cu–magnetite (32 wt%) deposit (Q = –67 C cm^{-2}) obtained at –67 mA cm^{-2} from the same solution of Fig. 2, 15 °C, ω = 60 rpm, magnet. (**B**) EDS spectrum obtained by spotting on an embedded particle

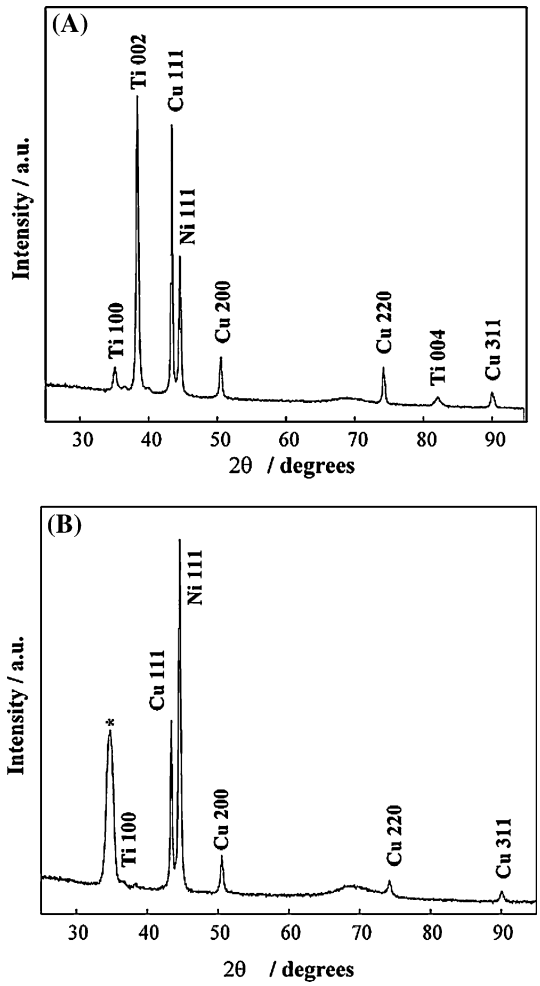

Fig. 6 X-ray diffractograms of deposits obtained from 0.5 mol dm^{-3} $CuSO_4$ + 0.2 mol dm^{3} H_2SO_4 + 1 g dm^{-3} DTAC + x g dm^{-3} Fe_3O_4 solution at 15 °C, ω = 60 rpm, magnet. Pulse-plating method, E_c = –850 mV, t_c = 8 s, E_a = 200 mV, t_a = 1 s. (**A**) x = 0, Q = –4.3 C cm^{-2}. (**B**) x = 50, Q = –25 C cm^{-2}

measured for both on-the-substrate and free-of-substrate composites. When the deposits were removed from the substrate, the coatings were placed parallel to the magnetic field so as to register the magnetic response. Other samples over the silicon-based substrate were also magnetically analysed.

Figure 7A shows the magnetic responses for both electrodeposited copper and copper–magnetite coatings after removing the layers from the substrate. A hysteresis curve was obtained even for coatings with low magnetite percentages whereas the typical diamagnetic behaviour is observed for pure-copper films.

Figure 7B shows M vs. H curves for the silicon-seed layer and copper–magnetite coatings with different compositions on the substrate. The magnetic response exhibited by the substrate (curve a) was due to the presence of nickel seed-layer. The magnetization measurement for copper magnetite coating revealed a ferromagnetic behaviour (curves b, c). A gradual increase in the magnetization of saturation was observed for coatings when magnetite percentage was higher. At a fixed composition, the magnetic response for composites was not dependant on the preparation technique.

Atomic force microscopy (AFM) images revealed clear differences in topography between the copper deposit (Fig. 8A) and the copper–magnetite composite (Fig. 8B). Moreover, the MFM phase images for the composite (Fig. 8D) exhibited a clear enhancement of the phase signal which was not observed for the corresponding to the copper deposit (Fig. 8C). In spite of a slight topography contribution, MFM profiles display

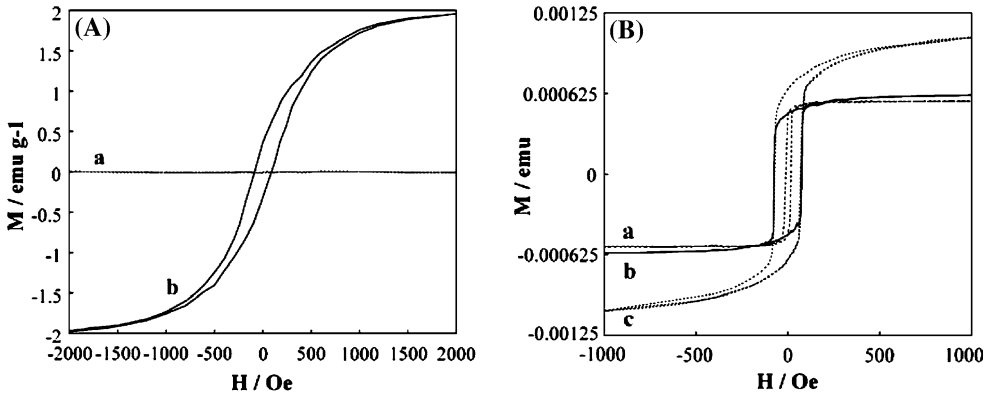

Fig. 7 (**A**) Magnetization curves of (a) copper deposit (Q = –10 C cm^{-2}) obtained at –15 mA cm^{-2} from a 0.5 mol dm^3 $CuSO_4$ + 0.2 mol dm^3 H_2SO_4 + 1 g dm^{-3} DTAC solution at 15 °C, ω = 60 rpm, magnet. (b) Copper–magnetite (5 wt%) composite (Q = –28 C cm^{-2}) obtained at –30 mA cm^{-2} from a 0.5 mol dm^{-3} $CuSO_4$ + 0.2 mol dm^{-3} H_2SO_4 + 1 g dm^{-3} DTAC + 25 g dm^{-3} Fe_3O_4 solution at 15 °C, ω = 60 rpm, magnet. (**B**) Magnetization curves of (a) Si/Ti/Ni substrate, (b) Si/Ti/Ni–Cu–magnetite (8 wt%) composite (Q = –18 C cm^{-2}), obtained by pulse-plating at E_c = –850 mV, t_c = 8 s, E_a = 200 mV, t_a = 1 s, from a 0.5 mol dm^{-3} $CuSO_4$ + 0.2 mol dm^{-3} H_2SO_4 + 1 g dm^{-3} DTAC + 50 g dm^{-3} Fe_3O_4 solution, 15 °C, ω = 60 rpm, magnet. (c) Si/Ti/Ni–Cu–magnetite (14 wt%) composite (Q = –10 C cm^{-2}), obtained at –850 mV from a 0.5 mol dm^{-3} $CuSO_4$ + 0.2 mol dm^{-3} H_2SO_4 + 1 g dm^{-3} DTAC + 25 g dm^{-3} Fe_3O_4 solution, 15 °C, ω = 60 rpm, magnet

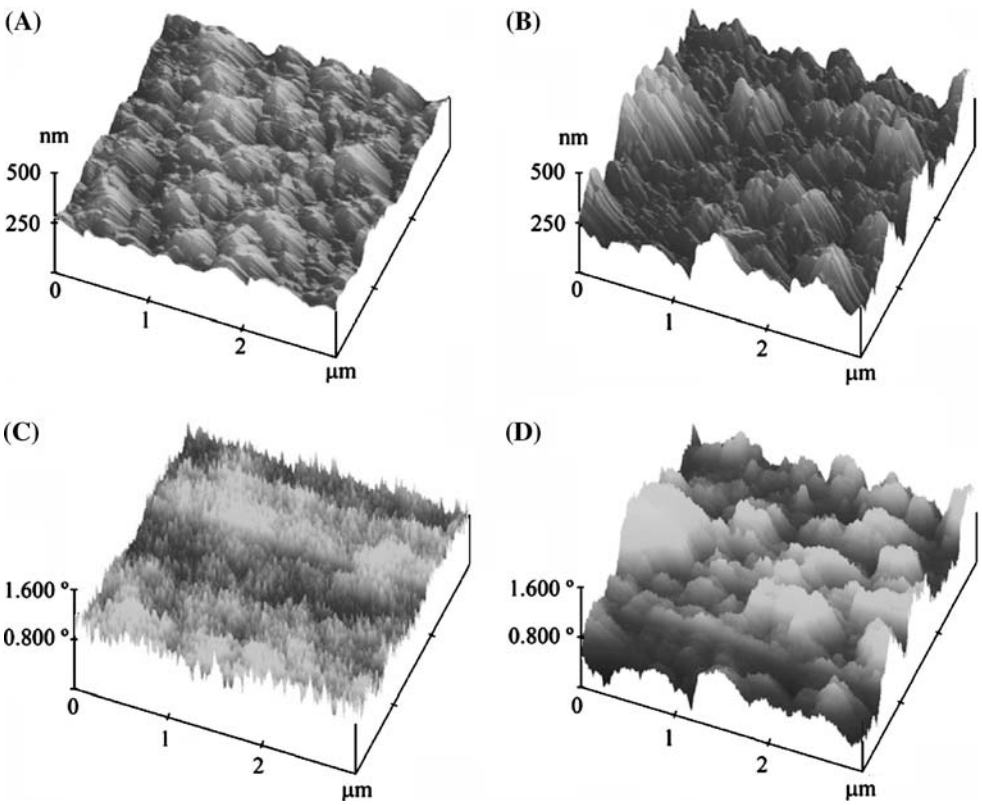

Fig. 8 AFM pictures corresponding to (**A**) copper deposit obtained from a 0.5 mol dm^{-3} $CuSO_4$ + 0.2 mol dm^{-3} H_2SO_4 + 1 g dm^{-3} DTAC solution at –850 mV, Q = –6.7 C cm^{-2}, 15 °C, ω = 60 rpm, magnet. (**B**) Cu–magnetite composite (17 wt% Fe_3O_4) from same bath with 25 g dm^{-3} Fe_3O_4 at –850 mV, Q = –30 C cm^{-2}, 15 °C, ω = 60 rpm, magnet. (**C** and **D**) are MFM phase images for the same samples

clearly an intensification of phase for the composite displaying a magnetic response attributable to the magnetite. In contrast, the phase profile corresponding to the copper deposit is nearly constant with no clear intensification of phase signal across the section.

4 Conclusions

The magnetic properties of copper can be clearly modified by means of electrodeposition of magnetite in plated copper. Electrodeposition is a useful method to

incorporate nanometric magnetite particles during copper growth, leading to copper–magnetite composites with different magnetite percentages. The magnetic properties of the composite can be modulated as a function of the magnetite incorporation.

The use of a cationic surfactant is crucial to induce significant particle incorporation. The best conditions for increasing magnetite incorporation are low temperature and low DTAC concentration, with moderate stirring. Magnetite incorporation is enhanced when using a magnetic field. Potentiostatic, galvanostatic or pulse-plating methods are adequate for magnetite incorporation. A high magnetite percentage (15–30 wt%) can be attained. Magnetite is uniformly distributed both on the surface and in depth, as observed by FE-SEM micrographs. Incorporation of nanometric particles of Fe_3O_4 leads to composites with ferromagnetic behaviour. MFM technique allows detection of magnetic behaviour of deposits due to the magnetite in the copper matrix.

Acknowledgments The authors thank Josep M. Montero-Moreno, the Serveis Cientificotècnics (Universitat de Barcelona), and the Servei de Magnetoquímica (Universitat de Barcelona) for the use of their equipment. This paper was supported by contract MAT 2003-09483-C02-01 from the *Comisión Interministerial de Ciencia y Tecnología (CICYT)*.

References

1. Han BQ, Huang JY, Zhu YT, Lavernia EJ (2006) Scr Mater 54:1175
2. Suryanarayana BC (2005) Adv Eng Mater 7:983
3. Curulli A, Valentini F, Padeletti G, Viticoli M, Caschera D, Palleschi G (2005) Sens Actuators B 111–112:441
4. Vaseashta A, Dimova-Malinovska D (2005) Sci Technol Adv Mat 6:312
5. Avramova I, Stefanov P, Nicolova D, Stoychev D, Marinova Ts (2005) Comp Sci Technol 65:1663
6. Pardavi-Horvath M, Takacs L (1993) J Appl Phys 73:6958
7. Bader SD (2002) Scr Mater 47:527
8. Dobrzanski LA, Drak M (2004) J Mater Process Technol 157–158:650
9. Arruebo M, Galan M, Navascues N, Carlos T, Marquina C, Ibarra MR, Santamaria S, (2006) Chem Mater 18:1911
10. Pardavi-Horvath M, Takacs T (1995) Scr Metal Mater 33:1731
11. Caizer C, Popovici M, Savii C (2003) Acta Mater 51:3607
12. Mandal K, Chakraverly S, Pan Mandal S, Agudo P, Pal M, Chakravorty D (2002) J Appl Phys 92:501
13. Hayashi N, Toriyama T, Wakabayashi H, Sakamoto I, Okada T, Kuriyama K (2002) Surf Coat Technol 158:193
14. Shull RD, Atzmony U, Shapiro AJ, Swartendruber LJ, Bennett LH, Green WJ, Moorjani K (1998) J Appl Phys 63:4261
15. Guan S, Nelson BJ, Vollmers K (2004) J Electrochem Soc 151:C545
16. Guan S, Nelson BJ (2005) Sens Actuators A 118:307
17. Guan S, Nelson BJ (2005) J Magn Magn Mater 292:49
18. Kim SK, Yoo HJ (1988) Surf Coat Technol 108–109:564
19. Pourroy G, Valles-Minguez A, Dintzer T, M. Richard-Plouet (2001) J Alloys Compd 327:267
20. Mugnier E, Pasquet I, Barnabé A, Presmanes L, Bonningue C, Tailhades P (2005) Thin Solid Films 493:49